Atmospheric Environment 185 (2018) 168–179

Contents lists available at ScienceDirect

Atmospheric Environment

journal homepage: www.elsevier.com/locate/atmosenv

Effect of weakened diurnal evolution of atmospheric boundary layer to air pollution over eastern China associated to aerosol, cloud – ABL feedback

Wenjun Qu[a,*], Jun Wang[b,**], Xiaoye Zhang[c,***], Yaqiang Wang[c], Shanhong Gao[a], Chuanhu Zhao[a], Linyuan Sun[a], Yang Zhou[a], Wencai Wang[a], Xiaohuan Liu[d], Huiqin Hu[a], Fei Huang[a]

[a] Physical Oceanography Laboratory/CIMST, Ocean University of China and Qingdao National Laboratory for Marine Science and Technology, Qingdao, China
[b] Center for Global and Environmental Research & Department of Chemical and Biochemical Engineering, University of Iowa, Iowa City, USA
[c] Chinese Academy of Meteorological Sciences, China Meteorological Administration, Beijing, China
[d] Lab of Marine Environmental Science and Ecology, Ministry of Education, Ocean University of China, Qingdao, China

ARTICLE INFO

Keywords:
Air pollution
Aerosol loading
Cloud cover
Atmospheric boundary layer stability
Diurnal temperature range
Eastern China

ABSTRACT

Upon the effect of atmospheric stability on air pollution, this study highlights the weakened diurnal evolution of atmospheric boundary layer (ABL), which is crucial to the formation of regional fog-haze and air pollution episodes over eastern China (ECN). The decrease of atmospheric visibility (Vis) during 1973–2012 is found to be related to the more stable ABL with weakened diurnal evolution that is characterized by a concurrent weakening of surface wind, a decrease in ABL height, and a reduction of diurnal temperature range (DTR, – 0.26 and – 0.092 °C/10-years in the winter and summer, respectively). With a general synchronous variation, the increase in both aerosol loading and cloud cover might work in concert to reduce solar radiation reaching the surface, stabilize ABL and weaken the diurnal ABL evolution, thereby weakening the turbulent mixing of pollutants and enhancing air pollution. This conjecture of "aerosol, cloud – ABL – air pollution" feedback, with particular emphasis on the effect of cloud (in addition to the effect of aerosol) on the ABL evolution, is supported by our analysis of 40 years trends in the cloud, Vis and DTR from surface observation, the aerosol optical depth from MODIS, and the validated MERRA-2 reanalysis aerosol, cloud and boundary layer height (by surface observation and routine radiosonde sounding). Regarding the linkage between fog-haze and diurnal evolution of the ABL, the result emphasizes the effect of a *persistent high* relative humidity (RH), which is found to be important to the formation of regional persistent fog-haze episodes and must be carefully considered in future study. Therefore, a chain of processes is suggested to interpret the occurrence of regional persistent fog-haze episodes over ECN. First, during a polluted day, because of aerosol radiative effects, the high ABL stability and high RH can persist throughout the day, and consequently, favoring the accumulation of pollutants as well as the secondary formation and hygroscopic growth of aerosol. Second, the maintenance of such more stable, humid and polluted ABL is in contrast to a clear day when the ABL is more convective in the afternoon and facilitates the diffusion and dilution of pollutants. Third, under a persistent stable synoptic system, the increase of air pollution associated with the weakened diurnal evolution of ABL due to the "aerosol, cloud – ABL – air pollution" feedback, as described above, can be further strengthened, thereby renders more persistent and severe air pollution events. The DTR variation in relationship with the aerosol, cloud, ABL and air pollution is also discussed.

1. Introduction

The global deterioration of air quality and the increase in atmospheric particulate matter (PM) concentrations have been attributed to the increase in anthropogenic emissions and more frequent stagnant weather conditions; the latter is believed to be part of large-scale climate change that has occurred over the past several decades and is likely to continue as the average global temperature increases (Jacob and Winner, 2009; Niu et al., 2010; Yan et al., 2011; Chin, 2012; Zhu et al., 2012; Qu et al., 2013, 2015a; Yin and Wang, 2015; Wang and Chen, 2016; Zhang et al., 2016).

The increase in aerosol loading and the change in weather condition also impact processes in the atmospheric boundary layer (ABL), as aerosols can alter atmospheric radiative transfer (either directly or indirectly by modifying cloud properties), and weathers can influence the ABL properties. Similar to the self-trapping mechanism of smoke

* Corresponding author.
** Corresponding author.
*** Corresponding author.
E-mail addresses: quwj@ouc.edu.cn (W. Qu), jun-wang-1@uiowa.edu (J. Wang), xiaoye@cma.gov.cn (X. Zhang).

https://doi.org/10.1016/j.atmosenv.2018.05.014
Received 1 November 2017; Received in revised form 7 May 2018; Accepted 8 May 2018
Available online 09 May 2018
1352-2310/ © 2018 Elsevier Ltd. All rights reserved.

Table 1
The variables and data used in this study. Refer to section 2 for the full name of the abbreviation that describes the data source, and to the acknowledgments for data availability.

Variable	Duration	Location	Source	Description
Vis (visibility) Wind speed T (daily air temperature) T_{max} (daily maximum air temperature) T_{min} (daily minimum air temperature) DTR (diurnal temperature range, defined as T_{max}–T_{min})	1973–2012	China	GSOD	Daily surface weather records from 354 Chinese stations; 136 stations over eastern China (ECN).
Cloud cover (the total lowest cloud cover) Air temperature	1973–2012	China	Daily 8 times surface weather records	00, 03, 06, 09, 12, 15, 18, 21 UTC; 427 Chinese stations, 172 stations over ECN.
AOD (aerosol optical depth) CF (cloud fraction)	2000–2016	110–120° E, 20–40° N	MODIS Terra	MOD08_M3 v6; 1° × 1° grid.
BLH (planetary boundary layer height) Surface incoming shortwave flux The extinction AOD Surface mass concentration	1980–2016	110–120° E, 20–40° N	NASA MERRA-2	0.5° × 0.625° grid; the surface incoming shortwave flux to reflect solar radiation; the extinction AOD, the surface mass concentration for the total aerosol and the major aerosol components.
RH (relative humidity)	2000–2014	110–120° E, 20–40° N	NCEP reanalysis	2.5° × 2.5° grid; at 1000 hPa, 925 hPa and 850 hPa.
Air temperature	1979–2016	110–120° E, 20–40° N	ECMWF reanalysis	1.0° × 1.0° grid; surface.
$PM_{2.5}$ concentration	Dec, 2016–Jan, 2017	Beijing, China	MEPC	Hourly average.

proposed for fires in the United States of America (USA; Robock, 1988; Wang and Christopher, 2006), Quan et al. (2013) used field observations of the ABL and measurements of air pollutants to suggest a possible positive feedback between aerosols and the ABL during pollution episodes in Tianjin, China. More aerosol loading is believed to result in a reduction in solar radiation (SR) reaching the surface, stabilizing the ABL and creating a positive feedback loop in which “more aerosol loading → more stable ABL → enhanced accumulation of pollutants within the ABL → more polluted and hazier atmosphere” (Zhang et al., 2013). A Weather Research and Forecast (WRF) – Community Multi-scale Air Quality (CMAQ) simulation study by Xing et al. (2015) identified the aerosol direct radiative effects (DRE) on surface air pollution and on the daytime temperature range, and found the largest magnitude of DRE under high-pollution conditions. A theoretical analysis also reported a more effective aerosol – ABL feedback at higher PM loading, which enhances air pollution (Petäjä et al., 2016). The intensification of aerosol pollution in Beijing was also linked to the feedback with surface SR and winds (Yang et al., 2016). Xing et al. (2016) found that the deterioration of the air quality due to aerosol cooling on the surface temperature and the modulation of atmospheric dynamics (resulting from increased stability) could complicate the evaluation of related health impacts. Using a two-way coupled WRF-CMAQ model, Wang et al. (2017a) separated the impact pathways of the aerosol direct effects on the air quality, and found that the maximum impacts on vertical diffusion occurred in the morning and evening and the maximum impacts on secondary reactions and dry deposition occurred at noon. On the other hand, Wang et al. (2013) and Ding et al. (2016) also highlighted the adverse impact of absorptive aerosols on air quality through heating the air and stabilizing the atmosphere. Such feedbacks, while conceptually understood, still require further verification and clarification for the exact mechanisms via long-term observational data. The possible effect of clouds on the ABL process and air pollution also must be investigated.

The severe air pollution and fog-haze episodes over eastern China (ECN), a global major polluted area, have received considerable attention (Zhao et al., 2013b; Zhang et al., 2013; Sun et al., 2014; Zhang et al., 2014). Statistics show that the annual averaged $PM_{2.5}$ concentration in central-eastern China reached over 100 μg m^{-3} (in some regions even over 150 μg m^{-3}), and only 4.1% of the Chinese cities attained the annual average standard of 35 μg m^{-3} in 2013 (Wang et al., 2017b). Regarding the adverse impact of air pollution on human health and life, $PM_{2.5}$ (the particulate matter with diameter < 2.5 μm)-related premature mortality in East Asia was found to increase by 21% from 1990 to 2010 (Wang et al., 2016). Studies over ECN did identify *a possible synchronous stabilization of the atmosphere and increase of the haze event*; for example, the atmospheric visibility (Vis) decline over ECN has been partially attributed to more frequent stagnant and humid weathers, which is associated with the strengthened and westward-extended western Pacific subtropical high in the summer (Qu et al., 2013) and fewer wintertime cold waves (CWs) and cold air activities (Qu et al., 2015a) since the 1970s. To continue the progress made in past studies toward a full understanding of the “aerosol, cloud – ABL – air pollution” feedback over ECN, this study investigates the possible relationship between aerosol pollution and the change in the ABL, especially the change in the low-level cloud cover, surface wind speed, boundary layer height (BLH) and diurnal temperature range (DTR). We especially focused on the climatology of the diurnal variation of parameters associated with the ABL evolution and on the factors favoring occurrence of the regional persistent fog-haze episodes (e.g., the persistent high relative humidity (RH), which has been previously considered less often).

2. Data

The data used in this study are provided in Table 1. The daily Vis (an average of the observations for the day of at least four records with an uncertainty of 0.1 km, China Meteorological Administration, 2003), wind speed, air temperature (T), daily minimum and maximum air temperature (T_{min} and T_{max}) and DTR (T_{max} – T_{min}) for the Chinese meteorological stations (Fig. 1a and e) were extracted from the Global Surface Summary of the Day (GSOD) database, the details of which were described in Qu et al. (2013). The 25th percentile Vis better

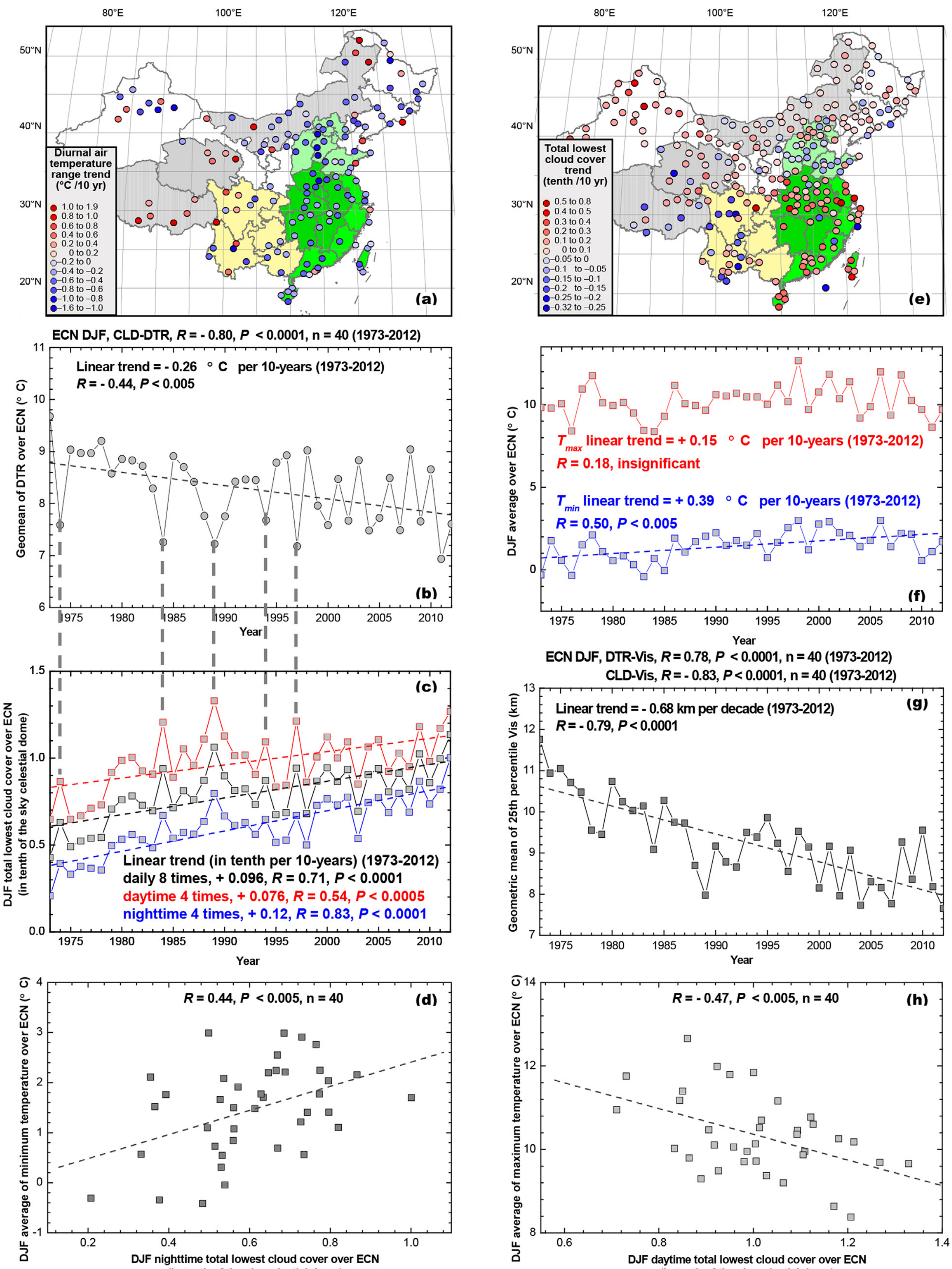

(caption on next page)

Fig. 1. (a) The trend of diurnal temperature range (DTR, °C/10yr) for the stations over China in winter from 1973 to 2012, all shown trends are significant at 95% confidence level. Partition of the area in China can be found in Qu et al. (2013, 2015a), and the area shaded with light green, green and dark green is eastern China (ECN). (b) Time series of the geometric mean of DTR (°C) over ECN in winter; the best linear fitting of the variable is presented, and the correlation between DTR and the total lowest cloud cover (CLD, tenth of the total celestial dome) is also presented at the panel top. (c), same as (b) but for CLD. (e), same as (a) but for the trend of CLD (tenth/10yr). (f), same as (b) but for the average daily minimum air temperature (T_{min}) and daily maximum air temperature (T_{max}, °C). (g), same as (b) but for the geometric mean of the 25th percentile Vis (km); the best linear fitting of the variable is presented, and the correlation between DTR and Vis as well as between CLD and Vis is also presented at the panel top. (d) Scatter plot of the average T_{min} (y-axis) with the nighttime CLD over ECN during 1973–2012; the best linear fitting line (dashed) between variables on the y-axis and x-axis is also shown. (h), same as (d) but for the average T_{max} (y-axis) with the daytime CLD.

reflects the trend of Vis (Qu et al., 2013) and air quality degradation; therefore, this value was used to assess the Vis variation. The RH from the NCEP (United States National Centers for Environmental Prediction) reanalysis data and the air temperature from the ECMWF (European Centre for Medium-Range Weather Forecasts) reanalysis data were also used.

The total lowest cloud cover and air temperature from the daily 8 times surface weather records were used to analyze the cloud cover and the temperature response. The total lowest cloud cover is the variable archived in the surface weather records, and was extracted to reflect the variation of low clouds (i.e., low-level cloud as termed in other studies). Low-level clouds were found to be especially effective at keeping the ground warm at night (Kukla and Karl, 1993) and reflecting the sunlight (Dai et al., 1999), thus causing the greatest change in DTR (Hansen et al., 1995). Therefore, the total lowest cloud cover is appropriate to use to evaluate the cloud impact on the DTR. Moreover, the daily 8 times records facilitated analysis of how the DTR responds to the diurnal variation of cloud cover.

The MODIS (MODerate resolution Imaging Spectroradiometer) Terra aerosol optical depth (AOD, MOD08_M3 V6) and cloud fraction (CF, MOD08_M3 V6) were used to evaluate the variation in AOD and CF. The AOD and CF products used were the most up-to-date versions with the highest confidence levels. The MERRA-2 (the Modern-Era Retrospective analysis for Research and Applications, Version 2) data of the planetary boundary layer height, surface incoming shortwave flux, extinction AOD and surface mass concentration of the major aerosol components were used in the analysis. MERRA-2 provides the latest atmospheric reanalysis of the modern satellite era that was produced by the National Aeronautics and Space Administration (NASA) Global Modeling and Assimilation Office (Gelaro et al., 2017). MERRA-2 is the first long-term global reanalysis to assimilate space-based observations of aerosols and represent their interactions with other physical processes in the climate system (https://gmao.gsfc.nasa.gov/reanalysis/MERRA-2/). (i) In MERRA-2, the dynamical core and physical parameterizations dealing with physical processes were performed using GEOS-5 (Goddard Earth Observing System model, version 5; Gelaro et al., 2017), a detailed description of which can be found in Molod et al. (2015). (ii) The MERRA-2 aerosol analysis uses the Goddard Aerosol Assimilation System (GAAS) to assimilate a quality-controlled AOD (from MODIS, Aerosol Robotics Network and other platforms) into the radiatively coupled GEOS-5/GOCART (Goddard Chemistry, Aerosol, Radiation, and Transport model) modeling system (Gelaro et al., 2017; Randles et al., 2017). The GOCART model is coupled with the GEOS atmospheric model to simulate the life cycles of five externally mixed aerosol species, including dust, sea salt, black carbon, organic carbon and sulfate, and to treat the sources, sinks, and chemistry of 15 externally mixed aerosol mass mixing ratio tracers, including dust (five non-interacting size bins), sea salt (five non-interacting size bins), hydrophobic and hydrophilic black and organic carbon (four tracers) and sulfate. Despite the fact that the aerosol properties (such as the vertical distribution, aerosol speciation, and absorption) are primarily determined by the underlying model physics and error covariance assumptions, the MERRA-2 aerosol reanalysis was found to have considerable skill in simulating numerous observable aerosol properties, and the AOD fields in MERRA-2 generally have both a high correlation and a low bias relative to independent (non-assimilated) sun photometer and aircraft observations (Gelaro et al., 2017; Randles et al., 2017). (iii) The assimilation of satellite radiances in MERRA-2 is performed using the CRTM (Community Radiative Transfer Model) version 2.1.3 (Gelaro et al., 2017), and a detailed description of this assimilation process is provided in Liu and Boukabara (2014). While the aerosol direct radiative effect (DRE) was critically assessed in Randles et al. (2017), the DRE efficiency for MERRA-2 was found to be within approximately 20% of the observational estimate (Yu et al., 2006).

To validate the quality of the cloud data, we compared the total lowest cloud cover from surface weather records over ECN with the CF derived from MODIS Terra (area averaged over 110–120° E, 20–40° N, which is the typical ECN region). The two variables varied synchronously in winter (December, January and February, DJF) during 2000–2012 with a significant correlation (R = 0.83, $P < 0.0005$; R = 0.88, $P < 0.0001$; R = 0.70, $P < 0.01$ for the daily, daytime and nighttime mean, respectively, n = 13), suggesting that both variables can reflect the variation of cloud cover well.

The hourly $PM_{2.5}$ concentration from the Ministry of Environment Protection of China (MEPC) and the hourly weather records for Beijing from December 2016 to January 2017 were also used to analyze the formation and persistence of fog-haze episodes associated with the evolution of the ABL.

3. Stabilizing and weakening of the diurnal evolution of the ABL associated with air pollution

The concurrent weakening of surface wind and decreasing of Vis over ECN in summer and winter have been reported in Qu et al. (2013, 2015a). The decline in Vis presumably reflects an aggravation of air pollution and an increase in aerosol loading, which is supported by the increasing trend in haze over ECN (Wang and Chen, 2016) and the increase in MERRA-2 AOD and surface mass concentrations of black carbon, sulfate and organic carbon (for details refer to the supplementary material).

Accompanied with the decline in Vis, the BLH calculated from MERRA-2 monthly mean shows a significant decrease (– 12 and – 19 m per 10-years, R = – 0.48 and – 0.49 in the winter and summer, respectively, $P < 0.005$, n = 33, Fig. 2a and b) during 1980–2012; the calculated BLH is also positively correlated with Vis in the winter (R = 0.70, $P < 0.0001$, n = 33) and summer (R = 0.46, $P < 0.01$, n = 33). Despite the overall decrease, the specific fluctuation of the MERRA-2 BLH before 1986 was further investigated by comparing it with the BLH calculated from daily radiosonde sounding observation at 00 UTC and 12 UTC for nine typical representative stations over different areas of ECN (http://weather.uwyo.edu/upperair/sounding.html). We calculated the BLH from the sounding data using the RH method (RH-BLH) and the potential temperature method (θ-BLH; Seidel et al., 2010). Consistent with the result from MERRA-2, a decreasing trend was identified in the BLH calculated from radiosonde sounding (for details refer to the supplementary material). Furthermore, there is a decreasing trend for the diurnal difference (defined as daily maximum minus minimum) of the 25th percentile Vis (– 0.33 and – 0.98 km per 10-years, Fig. 2c), the 75th percentile surface wind speed (– 0.14 and – 0.11 m/s per 10-years, Fig. 2d) and the cloud cover (– 0.063 and – 0.090 tenth per 10-years, Fig. 2e) in the winter and summer, respectively, during 1973–2012, implying a reduced diurnal contrast in Vis,

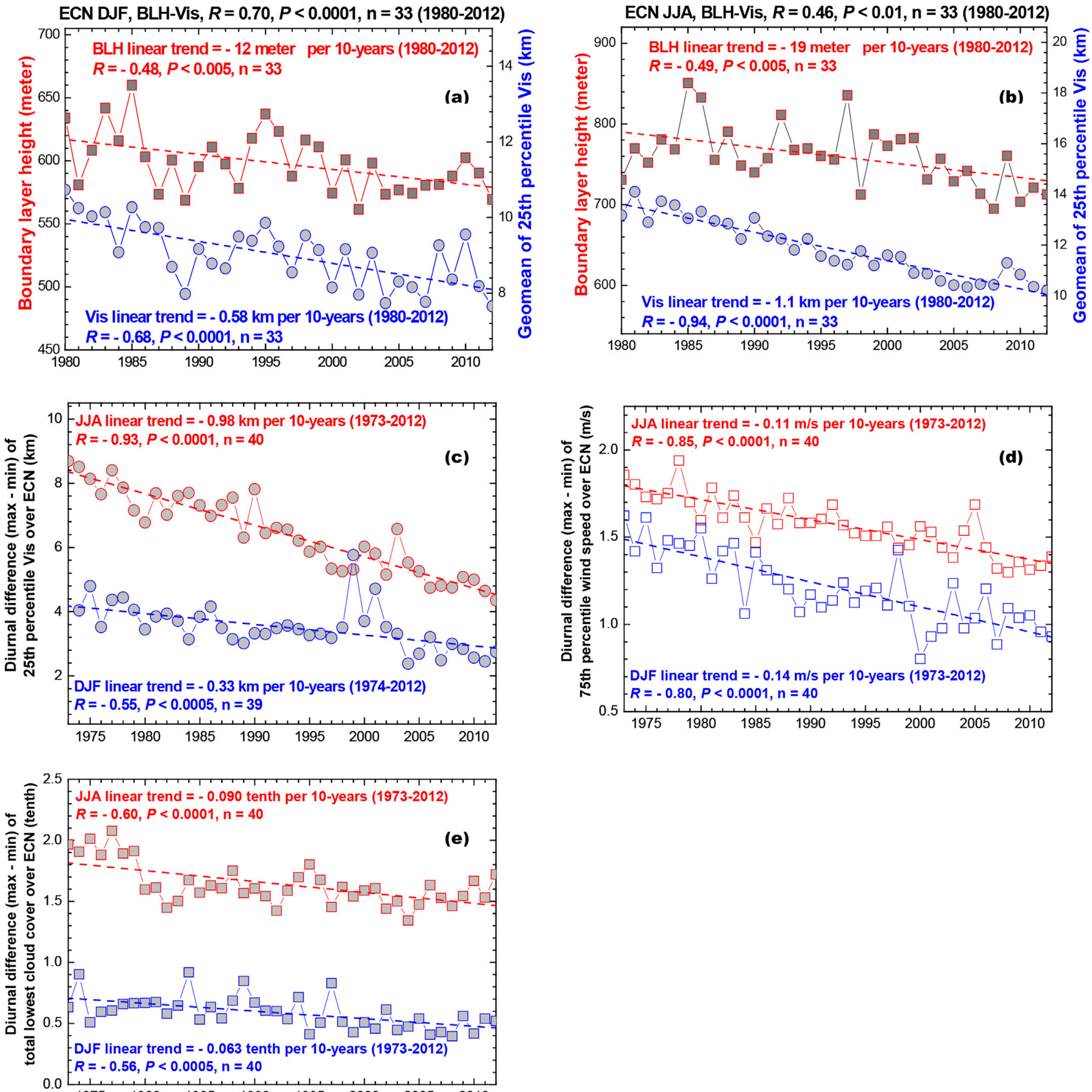

Fig. 2. Time series of the boundary layer height (BLH, meter) derived from the MERRA-2 model over 110–120° E, 20–40° N (the typical eastern China region, ECN) and the geometric mean of the 25th percentile visibility (Vis, km) over ECN (defined in Fig. 1) in (a) winter (December, January and February, DJF) and (b) summer (June, July and August, JJA) during 1980–2012; the best linear fitting of the variable is presented, and the correlation between Vis and BLH is also presented at the panels top. (c), (d) and (e), same as (a) but for the diurnal difference of the 25th percentile Vis (km), the 75th percentile wind speed (m/s) and the total lowest cloud cover (in tenth of the total celestial dome) over ECN in winter and summer during 1973–2012.

wind speed and cloud cover associated with the aggravation of air pollution over ECN.

The Weakening of the surface wind and decrease in the BLH suggests a more stable ABL, which favors the accumulation of pollutants near the surface; meanwhile a weakening diurnal evolution of the ABL was also reflected by the reduced diurnal contrast in Vis, wind speed, cloud cover and air temperature (to be discussed in section 4).

4. Decreased DTR – possible causes and relationship with air pollution

In contrast to the lack of a significant T_{max} trend (figures not shown), T_{min} increased at most stations over ECN (see the supplementary material) with an overall trend of +0.39 °C per 10-years (R = 0.50, $P < 0.005$, n = 40, Fig. 1f) in the winter during 1973–2012, which is approximately a factor of 2.5 of the trend in the T_{max} (+0.15 °C per 10-years, R = 0.18, insignificant, n = 40). This more significant increase in T_{min} (i.e., nighttime warming) over ECN, which is similar to that over the Tibetan Plateau (Liu et al., 2006) and over other areas of the globe (Alexander et al., 2006), can result in a declining DTR (Fig. 1a) with an overall trend of – 0.26 °C per 10-years (R = – 0.44, $P < 0.005$, n = 40, Fig. 1b) over ECN in the winter. This result is consistent with previous studies (Liu et al., 2004, 2016; Ye et al., 2010; Zhou and Ren, 2011; Wang et al., 2014). The decrease in DTR is another important feature of the more stable ABL over ECN in recent years in addition to the weakening of surface winds and the decrease in the BLH (see section 3).

The decrease in the DTR over China has been attributed to a decline in the solar irradiance (Liu et al., 2004), a decrease in the sunshine duration, and an increase in the surface soil moisture (Wang et al., 2014); the decrease in the solar irradiance and sunshine duration has been attributed to increased aerosol loading (Che et al., 2005; Wang et al., 2012). Wang and Christopher (2006) showed that the biomass burning particles over the USA can reduce the DTR by 0.31 °C and 0.26 °C near the smoke source and in downwind regions, respectively. Modeling over Asia during 1961–2005 (Liu et al., 2016) also suggested that anthropogenic aerosol forcing was mainly responsible for the decrease in the DTR, especially over ECN. Because the radiative effect of aerosols can influence the surface energy budget and consequently the DTR, the air pollution over ECN could be related to the variation in the DTR. A lower DTR is likely to reflect the effect of increased aerosol loading. Indeed, a close relationship was found between the DTR and Vis; both showed a decreasing trend over ECN in the winter (Fig. 1b and g) and correlated at R = 0.78 ($P < 0.0001$, n = 40, refer to Fig. 1g top). *The decrease in the DTR is associated with an increase in aerosol loading* (presumably reflected by the decreasing Vis, see the first paragraph in section 3) over ECN, and both changes resulted from the more stable atmosphere associated with more frequent fog-haze episodes in recent years (Qu et al., 2015a). This result is also consistent with the negative T_{min}-Vis correlation (R = – 0.58, $P < 0.0001$, n = 40); a warmer winter with less CW tends to favor low Vis and more frequent air pollution (Qu et al., 2015a).

In contrast to the synchronous decrease in the DTR and Vis (Fig. 1b and g), the cloud cover varied inversely with DTR (Fig. 1b and c) over ECN in the winter during 1973–2012. More specifically, the valley values of the DTR (Fig. 1b) are well corresponding to the peak values of cloud cover (Fig. 1c) for the winters of 1974, 1984, 1989, 1994 and 1997 (indicated by the dashed lines between Fig. 1b and c). A negative correlation was also identified between the DTR and cloud cover (R = – 0.80, $P < 0.0001$, n = 40, refer to Fig. 1b top), suggesting that the increase in cloud cover is another important factor that has resulted in the decrease in the DTR over ECN. This increasing trend of cloud cover is consistent with Xu (2012), who showed an increase in the low cloud cover to the south of the Yangtze River during 1960–2009. Inconsistent with the general increase in cloud cover over the entire ECN area, there was a decrease in cloud cover at many stations over the northern part of ECN (to the north of 35° N latitude, Fig. 1e). This decrease in the all-day cloud cover over northern ECN is an integrated result of the increase in cloud cover during the nighttime (13 stations increase versus 9 stations decrease, Fig. 3b) and the more significant decrease in cloud cover during the daytime (16 stations decrease versus 11 stations increase, Fig. 3a). The effect of this difference in the nighttime and daytime cloud cover on the DTR will be discussed in detail below.

To interpret the DTR change, the effects of greenhouse gases (GHGs), aerosols and clouds should be considered holistically (refer to the supplementary material for details). The direct radiative effect of GHGs on the DTR is negligible (Cao et al., 1992; IPCC, 2013) because GHGs are transparent to SR, and their effects on long-wave radiation (LWR) are equivalent during the daytime and nighttime and are thus equally efficient in affecting T_{max} and T_{min} (Kukla and Karl, 1993). On the other hand, the decrease in the SR and the decline of sunshine duration in China since the 1960s have been attributed to air pollution and increased aerosol loading (Che et al., 2005; Wang et al., 2012), suggesting the importance of considering aerosols in radiation balance and DTR variation.

Regarding the contribution of the increased aerosol loading and increased cloud cover (Fig. 1c and e) to the decrease in the DTR (Fig. 1a and b) over ECN, (i) the aerosol loading and cloud cover over ECN during 1973–2012, both of which showed a coherent increasing trend, tended to reduce the daytime SR, thus favoring a decrease in the T_{max} and, consequently a decrease in the DTR; (ii) the cloud cover was found to increase more rapidly during the nighttime (+0.12 tenth of the total celestial dome per 10-years), which is approximately 1.5 times that of the cloud cover during the daytime (+0.076 tenth/10-years, Fig. 1c). This difference may have resulted in a more significantly enhanced cloud effect upon trapping of the LWR at night (thus an increase in T_{min}) and contributed partially to the decrease in DTR.

Summarizing from the perspective of radiative forcing agents, (i) the direct effect of GHGs on the DTR is negligible, (ii) an increase in the aerosol loading (associated with more frequent fog-haze episodes over the region in recent years) can reduce the daytime SR, decrease the T_{max} and decrease the DTR, (iii) and the cloud influence on the DTR is a combined effect of reducing the daytime SR (associated with a decrease of T_{max}) and trapping the LWR with a daytime-nighttime difference, which is determined by the daytime and nighttime difference in cloud cover and consequently influences the T_{max} and T_{min}. Over the northern part of ECN, the trapping of LWR by the more significantly increased cloud cover during the nighttime (Fig. 3b) can result in more significantly enhanced nighttime warming than the daytime (with a general decrease in the cloud cover, Fig. 3a). Such enhanced nighttime warming (i.e., T_{min} increase) can also contribute to the decrease in the DTR (Fig. 1a).

Considering the daytime and nighttime effects separately, T_{min} is positively correlated with the nighttime cloud cover (R = 0.44, $P < 0.005$, n = 40, Fig. 1d) in the winter, whereas the T_{max} is negatively correlated with the daytime cloud cover (R = – 0.47, $P < 0.005$, n = 40, Fig. 1h). The opposite response of air temperature to cloud cover (positive during the nighttime due to trapping of the LWR, and negative during the daytime due to reducing of the SR) and the overall increasing trend of cloud cover over ECN (Fig. 1c) are consistent with the decrease in the DTR during 1973–2012 (Fig. 1b).

Fig. 4 illustrates that the air temperature trend at 5:00 a.m. local time (LT; the latest record before sunrise of the daily 8 times records) for the cloudy condition (cloud cover > 3/10, +0.52 °C per 10-years, R = 0.52, $P < 0.001$, n = 40, Fig. 4b) almost doubled that for the none/less cloud condition (cloud cover ≤ 3/10, +0.28 °C per 10-years, R = 0.30, $P < 0.1$, n = 40, Fig. 4a) over ECN in the winter during 1973–2012. The more significant *T* increase for the cloudy condition at night highlights the cloud effect on trapping of the LWR and nighttime warming. An analysis based on the ECMWF reanalysis data demonstrates that the trend of the surface air temperature at 5:00 a.m. LT in the winter increased from +0.12 °C per 10-years (insignificant) for the cloud fraction (CF) ranged in 0/10–2/10 to + 0.39 °C per 10-years (R = 0.45, $P < 0.005$, n = 38) for the CF ranged in 8/10–10/10 during 1979–2016 (refer to the supplementary material for details). The higher warming rate under a high-CF condition supports the above analysis based on the surface meteorological observations. The net total radiative forcing due to both direct and indirect aerosol effects at five rural USA sites during 2006–2011 was – 19 W/m^2 during the daytime in contrast to +16 W/m^2 averaged diurnally (Ten Hoeve and Augustine, 2015), which also suggests a positive nighttime radiative forcing.

Interestingly, the decreasing DTR is related to air pollution over ECN. A negative correlation was identified between Vis and cloud cover (R = – 0.83, $P < 0.0001$, n = 40, refer to Fig. 1g top); an increase in cloud cover (Fig. 1c) was found to occur concurrently with an increase in aerosol loading (presumably reflected by the decrease in Vis, as presented in Fig. 1g, which is associated with more frequent fog and haze episodes in recent years). Both the increase in cloud cover and the increase in aerosol loading tend to reduce the SR during the daytime

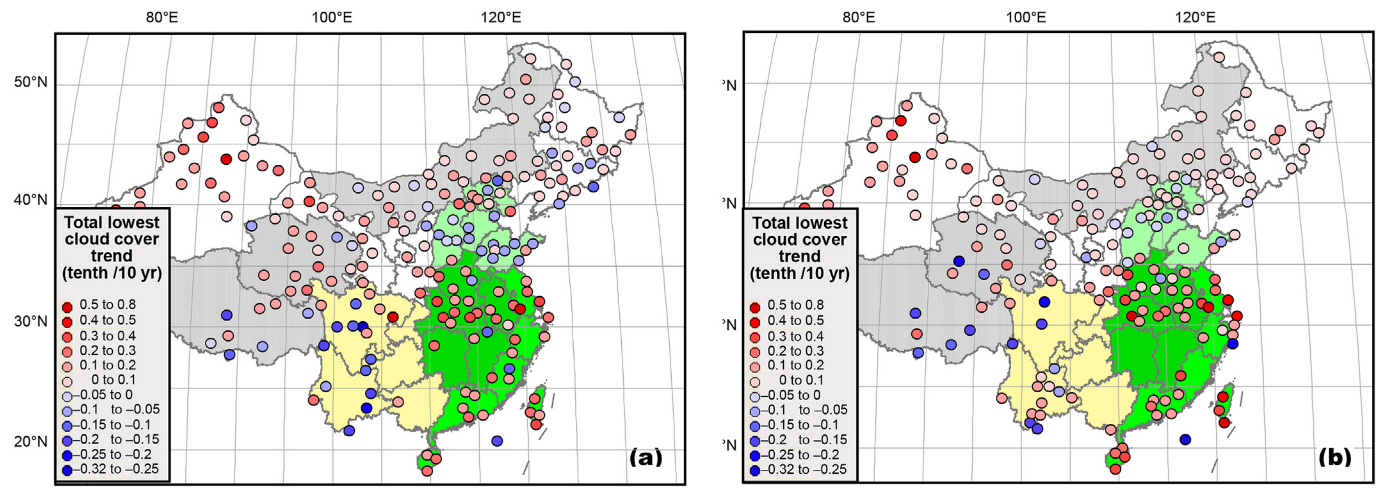

Fig. 3. (a) The trend of the daytime total lowest cloud cover (CLD, tenth of the total celestial dome) for the stations over China in winter (December, January and February, DJF) from 1973 to 2012, all shown trends are significant at 95% confidence level. Partition of the area in China can be found in Qu et al. (2013, 2015a), and the area shaded with light green, green and dark green is eastern China (ECN). (b), same as (a) but for the nighttime CLD.

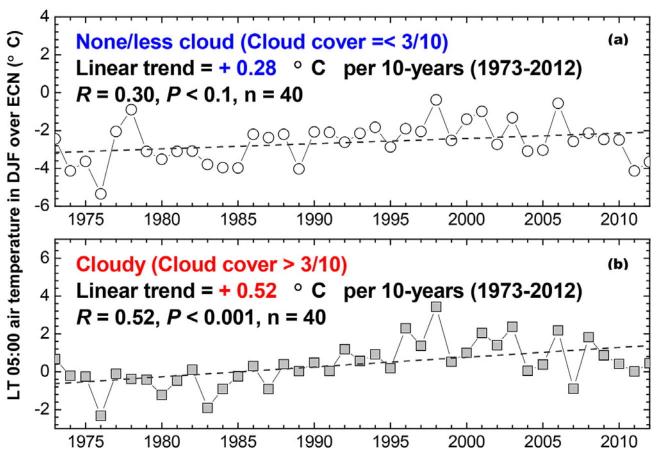

Fig. 4. The trend of air temperature (°C/10yr) at 5:00 a.m. LT (local time) over eastern China under (a) none/less cloud (cloud cover ≤ 3/10) and (b) cloudy (cloud cover > 3/10) conditions in winter from 1973 to 2012.

and result in a decrease in the T_{max}. On the other hand, nighttime warming, which is due to the more significantly enhanced cloud effect on trapping of the LWR by the more rapidly increased cloud cover at night (as discussed before), tends to result in an increase in the T_{min}. These effects thus result in a decrease in the DTR. This is a possible mechanism for how air pollution is linked to the decrease in the DTR.

The discussion above is mainly for the winter; the result for the summer is similar (refer to the supplementary material for details). The decreasing trend in the DTR for the summer (– 0.092 °C per 10-years, R = – 0.41, $P < 0.01$, n = 40) is smaller than that for the winter, and the summertime trend in the T_{min} (+0.28 °C) is approximately a factor of 1.5 of that in the T_{max} (+0.20 °C). The smaller difference between the trends of the T_{min} and T_{max} in the summer (compared to the winter) suggests a nighttime warming that is not as significant as that in the winter.

Considering the similar aerosol and cloud effect (for reducing the SR) and the additional cloud effect (for trapping the LWR) on the surface energy balance, the variations in the aerosols and clouds are important for their collaborative effect on the DTR, ABL evolution and air pollution, which will be discussed below.

5. Collaborative effect of aerosols and clouds

The time series of the AOD and CF derived from MODIS Terra in the winter months (December, January and February) during 2000–2012 show a similar increasing trend over ECN (Fig. 5a). A positive correlation exists between the winter monthly AOD and CF (R = 0.61, $P < 0.0001$, n = 39, Fig. 5b) during 2000–2012. This increase in cloud cover corresponding to the increase in AOD was also found in other area (Ten Hoeve and Augustine, 2015). However, considering the complicated and non-monotonic relationship between clouds and aerosols (Dagan and Chemke, 2016; Dagan et al., 2017), the synchronous variation of the AOD and CF over ECN, which does not necessarily reflect a causality between the increase in cloud cover and the increase in aerosol loading, is probably due to the covariation of the AOD and CF with specific meteorological factors, such as RH. Indeed, both the AOD and CF show a positive correlation with RH (R = 0.45 and 0.70, respectively, $P < 0.0001$, n = 39, Fig. 5c). The cloud formation is expected to enhance at an elevated RH (with a more abundant moisture supply); meanwhile, an elevated RH can also enhance the secondary formation and the hygroscopic growth of aerosols (Sun et al., 2013; Qu et al., 2015b), subsequently increasing the AOD. The latter process is also supported by the major hygroscopic component of the aerosols over ECN, in which the sulfate extinction AOD derived from MERRA-2 accounts for approximately 75% of the total aerosol AOD in the winter months during 1980–2012 (Fig. 5d). The long-term statistics here does not necessarily reflect any direct causal relationship between aerosols and clouds. However, further consideration of the specific chemical composition of aerosols and cloud condensation nuclei (CCN) should be helpful for investigating their relationship and interaction over different regions.

Because aerosols can serve as a source for CCN, a change in aerosols can affect the optical properties (Twomey, 1977; Wang et al., 2010, 2015), the extent (Albrecht, 1989) and thickness (Andreae et al., 2004; Altaratz et al., 2014) of the clouds as well as the precipitation (Koren et al., 2014). Kaufman and Koren (2006) reported that the elevated aerosol concentration was estimated to result in an increase in the average cloud cover by 5%. Gryspeerdt et al. (2016) found that the AOD-cloud cover relationship mainly resulted from the covariations of aerosol and cloud properties with the RH and convergence. Ten Hoeve and Augustine (2015) also highlighted the influence of the aerosol composition on the relationship between cloud cover and AOD. Although the exact mechanism and causality still must be further studied, the synchronous variation in the aerosol loading and the cloud cover over ECN can work in concert to affect the surface energy balance and

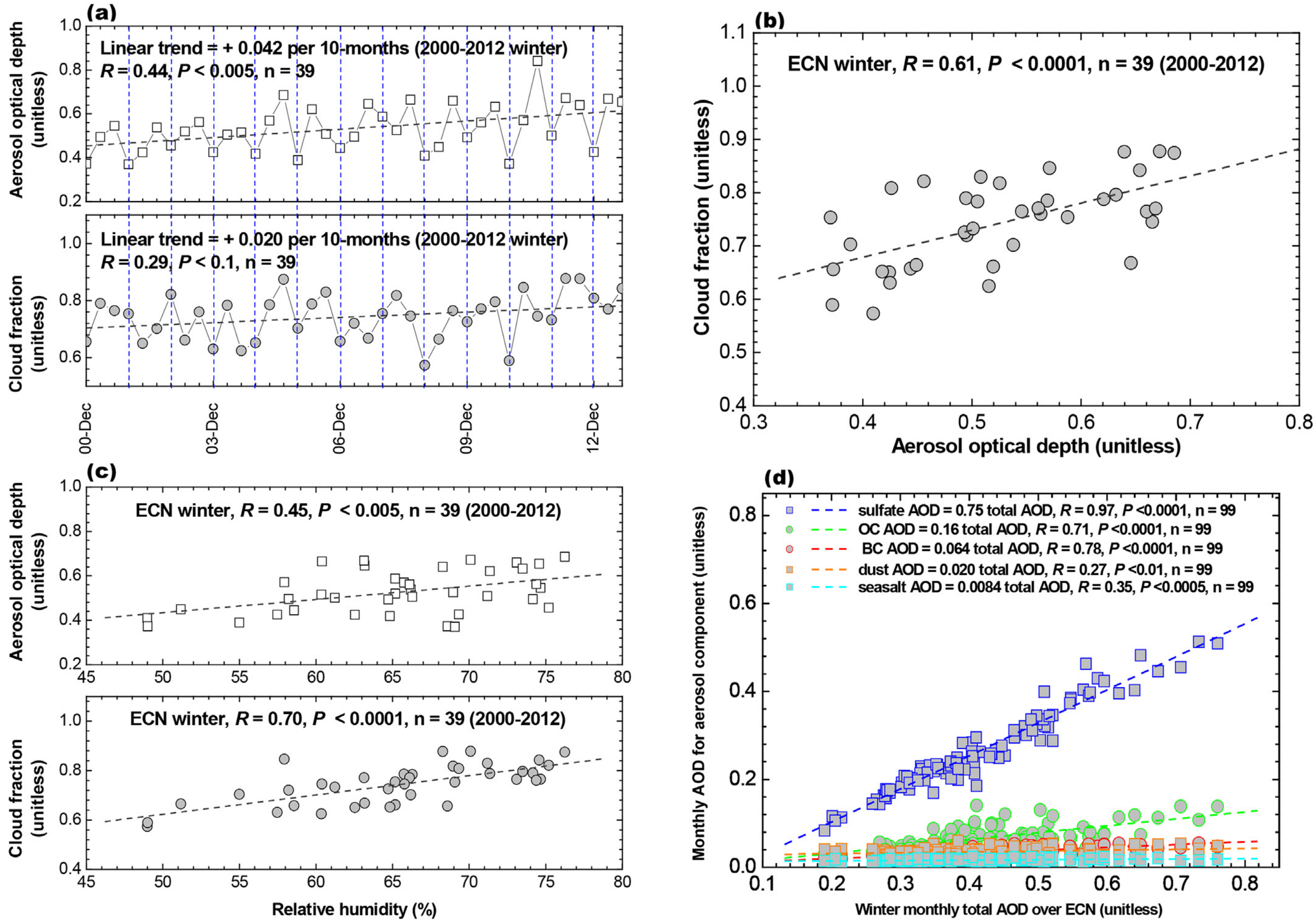

Fig. 5. (a) Time series of the monthly aerosol optical depth (AOD, unitless) and the monthly cloud fraction (CF, unitless, reflecting the cloud cover) from MODIS Terra over 110–120° E, 20–40° N (the typical eastern China region, ECN) in winter months (December, January and February) during 2000–2012. (b) Scatter plot of the monthly CF (y-axis) with monthly AOD over ECN in winter months during 2000–2012; the best linear fitting line (dashed) between variables on the y-axis and x-axis is also shown. (c), same as (b) but for monthly AOD (y-axis) and CF (y-axis) with the monthly mean relative humidity (RH, %) at 1000 hPa, 925 hPa and 850 hPa levels over ECN. (d), same as (b) but for the extinction AODs of the major aerosol components such as sulfate, organic carbon (OC), black carbon (BC), dust and seasalt derived from MERRA-2 (y-axis) with AOD of the total aerosol over ECN in winter months during 1980–2012.

ABL evolution, which consequently influence the DTR and air pollution in the region.

6. Effect of aerosols and clouds on the ABL evolution: possible mechanism for air pollution

According to the above discussion, the increased amount of aerosols is expected to reduce the SR reaching the surface, stabilize the ABL and favor the occurrence of air pollution (Quan et al., 2013; Zhang et al., 2013; Petäjä et al., 2016). Similarly, an increase in cloud cover will reduce the SR, leading to another possible positive feedback loop, such as "higher aerosol concentration and larger cloud fraction → SR reduction → cooling surface and more stable ABL → enhanced accumulation of pollutants and more polluted atmosphere", as supported by the synchronous variation in the AOD and cloud cover over ECN (section 5). A recent observational study of Nanjing, China (Zou et al., 2017) also found that high aerosol loading can significantly increase the ABL stability and efficiently reduce the BLH.

The effect of the increased aerosol loading and cloud cover on the SR reduction (which further affect the ABL stabilization and air pollution) can be validated by the decrease in the surface incoming shortwave flux (indicating SR) over ECN (– 2.2 and – 6.6 W/m^2 per 10-years, R = – 0.42 and – 0.79, $P < 0.05$ and < 0.0001 in the winter and summer, respectively, Fig. 6a and b) during 1980–2014, which is negatively correlated with the total aerosol extinction optical depth and the total lowest cloud cover in the winter (R = – 0.61 and – 0.85, $P < 0.0001$, Fig. 6c and e) and summer (R = – 0.70 and – 0.55, $P < 0.0001$, Fig. 6d and f).

A comparison of the diurnal variation of pollutants and meteorological factors between a fog-haze day and a normal day is helpful for understanding how the more stable and weakening diurnal evolution ABL contributes to the occurrence and long-durative persistence of air pollution episodes (Fig. 7). Analysis of the sounding observations (http://weather.uwyo.edu/upperair/sounding.html) for the fog and haze episodes in Beijing during December 11, 2016 to January 17, 2017 showed that an enhanced temperature inversion persisted during both nighttime and daytime on the fog-haze days and that the water vapor condensation height was reduced to as low as 100–200 m (figures not shown). During normal clear days (with no significant air pollution), a decrease in the $PM_{2.5}$ concentration, an increase in the surface wind speed (WDSP) and a decrease in the RH generally occurred in the afternoon with more convective ABL; in contrast, during the fog and haze days (H-1, December 17 to 21, 2016, and H-2, December 30, 2016 to January 7, 2017, when the air quality was reported as high-level pollution to severe pollution by MEPC, Fig. 8) the $PM_{2.5}$ concentration and RH generally remained at high levels (Fig. 8c and b) and were associated with a low WDSP (Fig. 8a) and a more stable ABL throughout the day. Therefore, (i) the general diffusion and dilution of pollutants

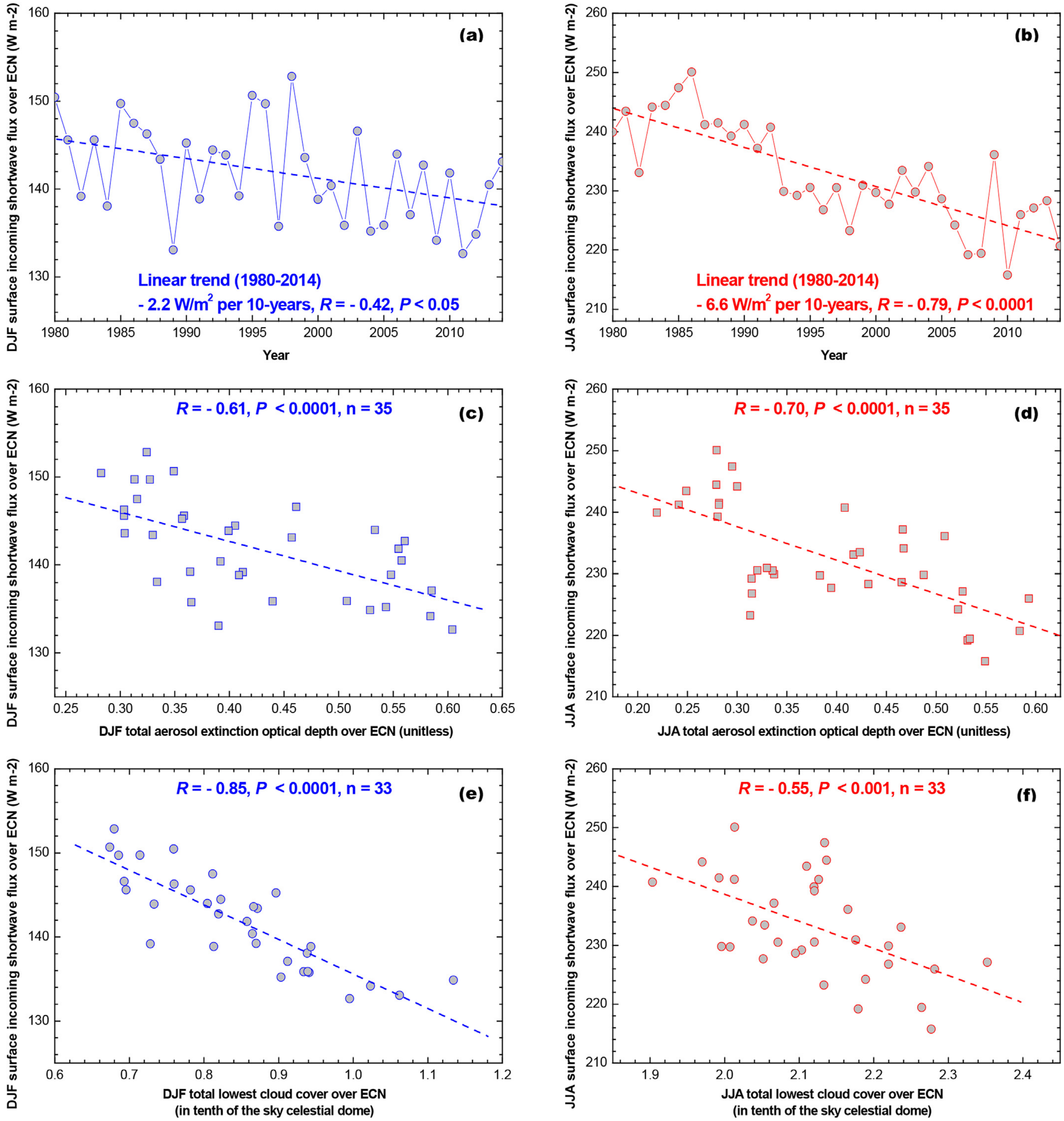

Fig. 6. Time series of the surface incoming short-wave flux (W m^{-2}) derived from the MERRA-2 model over 110–120° E, 20–40° N (the typical eastern China region, ECN) in (a) winter (December, January and February, DJF) and (b) summer (June, July and August, JJA) during 1980–2014. Scatter plot of the surface incoming short-wave flux (y-axis) with the extinction aerosol optical depth for the total aerosol (unitless) derived from MERRA-2 over ECN in (c) winter and (d) summer; the best linear fitting line (dashed) between variables on the y-axis and x-axis is also shown. (e) and (f), same as (c) and (d) but for the surface incoming short-wave flux with the total lowest cloud cover (in tenth of the total celestial dome).

that normally occur in the afternoon (accompanied with more efficient convection and turbulent mixing) on a clear day could weaken or disappear during fog-haze days, and this could be one reason for the persistence of air pollution episodes (Fig. 7). Consistently, Qu et al. (2015a) identified a lower afternoon BLH over ECN during a less CW influenced and more polluted winter. The second reason for the persistence of regional fog-haze episodes could be (ii) the maintenance of a high RH as well as an enhanced secondary formation and hygroscopic growth of aerosols (which are more efficient at a high RH; Sun et al., 2013; Qu et al., 2015b) throughout the day (Fig. 7). Indeed, during the fog and haze episodes (H-1 and H-2, Fig. 8), the RH was consistent throughout the day at a high level that was comparable or greater than 60% (Fig. 8b, e.g., during December 20–21, 2016, and January 1 and January 4–7, 2017); or the low RH (i.e., < 40%) duration (that might

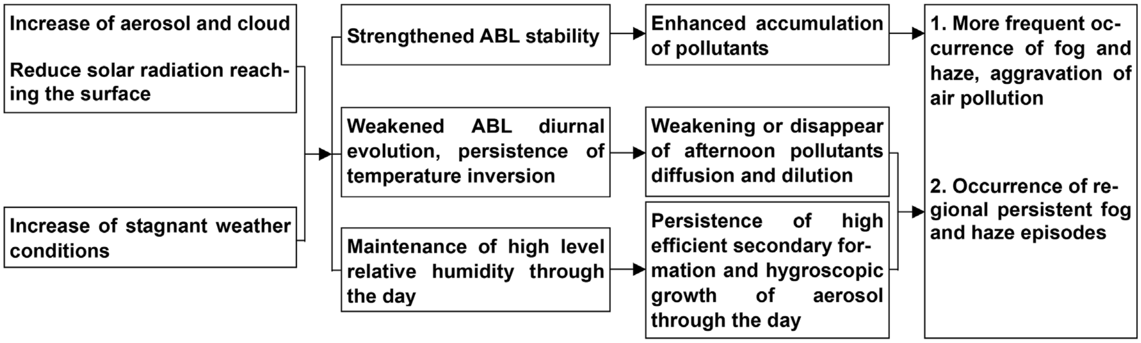

Fig. 7. A conceptual illustration about the effect of increased aerosol, cloud and more stagnant weather on the stability and diurnal evolution of atmospheric boundary layer (ABL), and consequently on the occurrence of regional persistent fog-haze episodes and aggravation of air pollution.

occur at noon and in the afternoon) became much less than that during the clear days, and could be reduced to less than 6 h (e.g., during December 17–19 and December 30–31, 2016, and January 2–3, 2017). Here 60% is the deliquescence point of aerosols, exceeding which hygroscopic growth becomes more efficient (Wang et al., 2008). To consider the hygroscopic growth, we calculated the ambient $PM_{2.5}$ concentration (abbreviated as APM25C, Fig. 8) using the IMPROVE (Interagency Monitoring of Protected Visual Environments) algorithm (http://vista.cira.colostate.edu/Improve/the-improve-algorithm/). The ambient concentration of sulfate and nitrate was calculated by multiplying the dry mass concentration of sulfate and nitrate (which is assumed to account for 37% of the $PM_{2.5}$ dry mass concentration according to Zhao et al., 2013a) by a hygroscopic growth factor *f(RH)* (http://vista.cira.colostate.edu/Improve/wp-content/uploads/2016/03/fRHOriginalIMPROVE.csv). The calculated ambient sulfate and nitrate concentration was subsequently added to the concentration of the other species to obtain the APM25C (Zhao et al., 2013a). Because *f(RH)* shows exponential growth with an increase of in RH (within the high RH range), the calculated APM25C varied beyond several orders of magnitude. To accommodate this feature and facilitate the comparison of the APM25C, the natural logarithm (Ln) was used here. A Ln (ambient $PM_{2.5}$ concentration) $>$ 5 during the pollution episodes (e.g., H-1 and H-2, Fig. 8d) suggests that the APM25C persisted at a high level (associated with aggravation of air pollution) during the fog-haze episodes in contrast to the low level of APM25C found during normal clear days. In a broader context, the increase in global surface specific humidity accompanied with warming (Dai, 2006) may enhance these processes and favor the occurrence and persistence of fog and haze episodes.

In summary, in contrast to normal clear days in which there is diffusion and dilution of pollutants and a decrease in RH that generally occurs with a more convective ABL in the afternoon, the ABL during fog-haze days shows less diurnal contrast, with a low WDSP, a high RH as well as a high dry and ambient $PM_{2.5}$ concentration persisting throughout the day. Thus, the maintenance of an atmospheric temperature inversion that is associated with a stable, shallow and humid

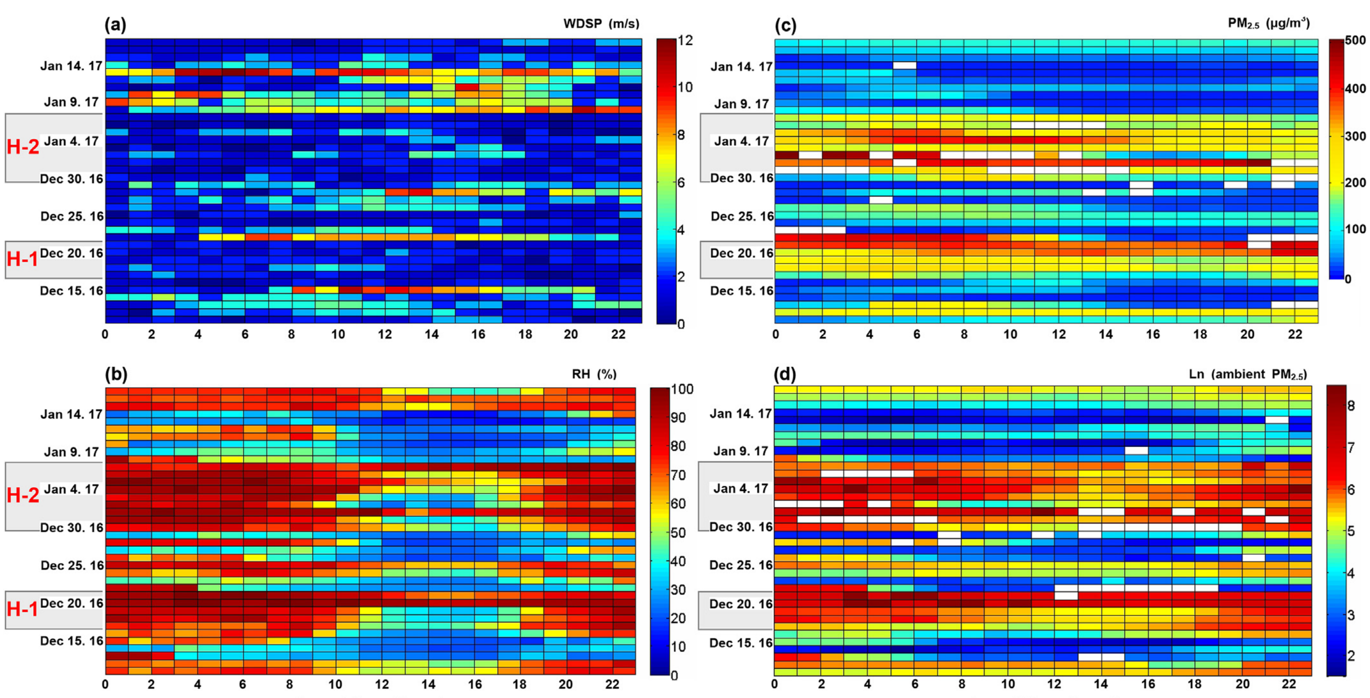

Fig. 8. Diurnal variation of the near surface (a) wind speed (WDSP, m/s), (b) relative humidity (RH, %), (c) $PM_{2.5}$ concentration reported by the Ministry of Environment Protection of China (MEPC), and (d) the natural logarithm (Ln) of the ambient $PM_{2.5}$ concentration in Beijing during December 11, 2016 to January 17, 2017; the cell filled with white indicates a missing value for the time. During this period, there were two persistent fog, haze and air pollution episodes during December 17 to 21, 2016 (H-1) and during December 30, 2016 to January 7, 2017 (H-2), accompanied with high $PM_{2.5}$ concentration, and the air quality was reported as high-level pollution to severe pollution by MEPC.

ABL with less diurnal variation ABL (under a specific stable synoptic system) is favorable for the formation and persistence of fog-haze and air pollution episodes.

7. Conclusions and discussion

Air pollution was found to be related to weakened diurnal evolution of the ABL, which was demonstrated by a concurrent decrease in the Vis and DTR over ECN in recent years. Accompanied with the aggravation of air pollution, an increase in both aerosol loading and cloud cover was identified, which can reduce the SR reaching the surface, stabilize the ABL and weaken the diurnal ABL evolution, thus favoring the occurrence of more severe and persistent fog-haze episodes. The negative T_{min}-Vis correlation and positive DTR-Vis correlation are consistent with the fact that a warmer winter with lower DTR and weaker ABL diurnal evolution is hazier than a colder winter with higher DTR and more dynamic ABL evolution. The weakened diurnal evolution of the ABL, which is characterized by a reducing diurnal contrast in *T*, Vis, wind speed and cloud cover, is important for air pollution aggravation over ECN and must be carefully considered.

Our comparison of the BLH from the MERRA-2 reanalysis data with the calculated RH-BLH and θ-BLH from sounding at nine typical stations over ECN generally supports a decrease in the BLH in the region. However, further investigation of the variation in the BLH with consideration of the frequency of atmospheric temperature inversions and the sounding observation is warranted to further clarify how the ABL evolution interacts with the regional air pollution over ECN in the context of increasing anthropogenic emissions and more frequent stagnant weather conditions in the region. Furthermore, the sounding data in China during the early years generally has coarse vertical resolution, and the surface-level records are occasionally missing, suggesting that more careful consideration should be taken, such as only considering the standard pressure level to reduce the uncertainty from the inconsistent vertical resolution during the study period. A combined systematic algorithm using adequate methods of the BLH calculation as suggested in Seidel et al. (2010) must be constructed for determining the BLH from the sounding observations and to subsequently evaluate the BLH variation over ECN.

On the other hand, measurements of the diurnal variation in aerosol composition for the secondary and hygroscopic species are also necessary to determine how the persistence of more efficient secondary formation and hygroscopic growth of aerosols contributes to the occurrence of regional persistent fog and haze episodes. The "aerosol, cloud – ABL – air pollution" feedback and the suggested mechanism of regional persistent fog-haze episodes, which are associated with the weakened diurnal evolution of the ABL, should be considered to improve regional air quality forecasts over ECN.

The increasing trend in $T_{\min}$ (+0.39 and + 0.28 °C per 10-years) is approximately a factor of 2.5 and 1.5 of that in the $T_{\max}$ (+0.15 and + 0.20 °C per 10-years) in the winter and summer, respectively, which resulted in a decrease in the DTR over ECN during 1973–2012. While the GHG warming is equivalent all day, the faster increase in the $T_{\min}$ and the decrease in the DTR are due to the following: (i) the counterbalance to GHG warming due to a reduction in the SR by aerosols and clouds, which is only effective during the daytime and slows down the increase in $T_{\max}$; (ii) the trapping of LWR with a greater nighttime magnitude by the more rapid increase in cloud cover at night versus the day (+0.12 versus + 0.076 tenth of the total celestial dome per 10-years in winter), which further increases $T_{\min}$. Compare with the daytime, the more rapid increase in cloud cover at night and the doubled warming trend at 5:00 a.m. LT for a cloud cover > 3/10 (against that for a cloud cover ≤ 3/10) highlights the nighttime cloud effect for trapping LWR (with a larger magnitude), favoring a more significant nighttime warming.

The concurrent decline in the DTR and Vis as well as the synchronous variation in the aerosols and clouds over ECN are unique in the global background; a preliminary inspection found different variations in the DTR and Vis over other global areas. The chemical composition and microphysical properties of the particles, fog droplets and CCN may play an important role in the cloud process as well as in the formation of fog-haze episodes. For different global areas with various aerosol components, the interaction between the air pollution with ABL stability and the diurnal evolution via the effect of a changing aerosol loading and cloud cover should be investigated specifically on a regional scale rather than on a global scale (as suggested by Chin et al. (2014)), which should be carefully considered in future modeling research.

Acknowledgments:

The GSOD data are available at ftp://ftp.ncdc.noaa.gov/pub/data/gsod; the NCEP reanalysis data are available at http://www.esrl.noaa.gov/psd/data/gridded/data.ncep.reanalysis.html; the daily 8 times weather records are available at http://www1.ncdc.noaa.gov/pub/data/noaa/; the AOD and CF from MODIS, the BLH and the extinction AOD, the surface mass concentration for aerosol components from MERRA-2 are available at http://giovanni.sci.gsfc.nasa.gov/giovanni/; the hourly surface $PM_{2.5}$ concentration in Beijing are available at http://datacenter.mep.gov.cn/.

We thank Prof. Ilan Koren from Weizmann Institute of Science for constructive discussion and the anonymous reviewer for help on the improvement of manuscript. This research is supported by National Key Project of MOST (2016YFC0203306), NSFC 41276009 and the Basic Scientific Research Progress of the Chinese Academy of Meteorological Sciences (2017Z011).

Appendix A. Supplementary data

Supplementary data related to this article can be found at http://dx.doi.org/10.1016/j.atmosenv.2018.05.014.

References

Albrecht, B.A., 1989. Aerosols, cloud microphysics, and fractional cloudiness. Science 245, 1227–1230.
Altaratz, O., Koren, I., Remer, L.A., Hirsch, E., 2014. Review: cloud invigoration by aerosols—coupling between microphysics and dynamics. Atmos. Res. 140, 38–60.
Alexander, L.V., Zhang, X., Peterson, T.C., Caesar, J., Gleason, B., Klein Tank, A.M.G., Haylock, M., Collins, D., Trewin, B., Rahimzadeh, F., Tagipour, A., Rupa Kumar, K., Revadekar, J., Griffiths, G., Vincent, L., Stephenson, D.B., Burn, J., Aguilar, E., Brunet, M., Taylor, M., New, M., Zhai, P., Rusticucci, M., Vazquez-Aguirre, J.L., 2006. Global observed changes in daily climate extremes of temperature and precipitation. J. Geophys. Res. 111http://dx.doi.org/10.1029/2005JD006290. D05109.
Andreae, M.O., Rosenfeld, D., Artaxo, P., Costa, A.A., Frank, G.P., Longo, K.M., Silva-Dias, M.A.F., 2004. Smoking rain clouds over the Amazon. Science 303, 1337–1342.
Cao, H.X., Mitchell, J.F.B., Lavery, J.R., 1992. Simulated diurnal range and variability of surface temperature in a global climate model for present and doubled CO_2 climates. J. Clim. 5, 920–943.
Che, H.Z., Shi, G.Y., Zhang, X.Y., Arimoto, R., Zhao, J.Q., Xu, L., Wang, B., Chen, Z.H., 2005. Analysis of 40 years of solar radiation data from China, 1961–2000. Geophys. Res. Lett. 32http://dx.doi.org/10.1029/2004GL022322. L06803.
Chin, M., 2012. Dirtier air from a weaker monsoon. Nat. Geosci. 5, 449–450.
Chin, M., Diehl, T., Tan, Q., Prospero, J.M., Kahn, R.A., Remer, L.A., Yu, H., Sayer, A.M., Bian, H., Geogdzhayev, I.V., Holben, B.N., Howell, S.G., Huebert, B.J., Hsu, N.C., Kim, D., Kucsera, T.L., Levy, R.C., Mishchenko, M.I., Pan, X., Quinn, P.K., Schuster, G.L., Streets, D.G., Strode, S.A., Torres, O., Zhao, X.-P., 2014. Multi-decadal aerosol variations from 1980 to 2009: a perspective from observations and a global model. Atmos. Chem. Phys. 14, 3657–3690.
China Meteorological Administration, 2003. Specifications for Surface Meteorological Observation (In Chinese). China Meteorological Press, pp. 151.
Dagan, G., Koren, I., Altaratz, O., Heiblum, R.H., 2017. Time-dependent, non-monotonic response of warm convective cloud fields to changes in aerosol loading. Atmos. Chem. Phys. 17, 7435–7444.
Dagan, G., Chemke, R., 2016. The effect of subtropical aerosol loading on equatorial precipitation. Geophys. Res. Lett. 43, 11048–11056. http://dx.doi.org/10.1002/2016GL071206.
Dai, A., Trenberth, K.E., Karl, T.R., 1999. Effects of clouds, soil moisture, precipitation, and water vapor on diurnal temperature range. J. Clim. 12 (8), 2451–2473.
Dai, A., 2006. Recent climatology, variability, and trends in global surface humidity. J. Clim. 19, 3589–3606.

Ding, A., Huang, X., Nie, W., Sun, J., Kerminen, V.M., Petäjä, T., Su, H., Cheng, Y., Yang, X., Wang, M., Chi, X., Wang, J., Virkkula, A., Guo, W., Yuan, J., Wang, S., Zhang, R., Wu, Y., Song, Y., Zhu, T., Zilitinkevich, S., Kulmala, M., Fu, C., 2016. Enhanced haze pollution by black carbon in megacities in China. Geophys. Res. Lett. 43, 287–2879. http://dx.doi.org/10.1002/2016GL067745.
Gelaro, R., McCarty, W., Suárez, M.J., Todling, R., Molod, A., Takacs, L., Randles, C.A., Darmenov, A., Bosilovich, M.G., Reichle, R., Wargan, K., Coy, L., Cullather, R., Draper, C., Akella, S., Buchard, V., Conaty, A., Silva, A.M.D., Gu, W., Kim, G.–K., Koster, R., Lucchesi, R., Merkova, D., Nielsen, J.E., Partyka, G., Pawson, S., Putman, W., Rienecker, M., Schubert, S.D., Sienkiewicz, M., Zhao, B., 2017. The modern-era retrospective analysis for research and applications, version 2 (MERRA-2). J. Clim. 30 (14), 5419–5454.
Gryspeerdt, E., Quaas, J., Bellouin, N., 2016. Constraining the aerosol influence on cloud fraction. J. Geophys. Res. 121, 3566–3583. http://dx.doi.org/10.1002/2015JD023744.
Hansen, J., Sato, M., Reudy, R., 1995. Long-term changes of the diurnal temperature cycle: implications about mechanisms of global climate change. Atmos. Res. 37, 175–209.
IPCC, 2013. In: Stocker, T.F., Qin, D., Plattner, G.-K., Tignor, M., Allen, S.K., Boschung, J., Nauels, A., Xia, Y., Bex, V., Midgley, P.M. (Eds.), Climate Change 2013: the Physical Science Basis, Contribution of Working Group I to the Fifth Assessment Report of the Intergovernmental Panel on Climate Change. Cambridge University Press, Cambridge, United Kingdom and New York, NY, USA, pp. 1535.
Jacob, D.J., Winner, D.A., 2009. Effect of climate change on air quality. Atmos. Environ. 43, 51–63.
Kaufman, Y.J., Koren, I., 2006. Smoke and pollution aerosol effect on cloud cover. Science 313, 655–658. http://dx.doi.org/10.1126/science.1126232.
Koren, I., Dagan, G., Altaratz, O., 2014. From aerosol-limited to invigoration of warm convective clouds. Science 344, 1143–1146.
Kukla, G., Karl, T.R., 1993. Nighttime warming and the greenhouse effect. Environ. Sci. Technol. 27 (8), 1468–1474.
Liu, B.H., Xu, M., Henderson, M., Qi, Y., Li, Y.Q., 2004. Taking China's temperature: daily range, warming trends, and regional variations, 1955–2000. J. Clim. 17, 4453–4462.
Liu, X., Yin, Z.-Y., Shao, X., Qin, N., 2006. Temporal trends and variability of daily maximum and minimum, extreme temperature events, and growing season length over the eastern and central Tibetan Plateau during 1961–2003. J. Geophys. Res. 111http://dx.doi.org/10.1029/2005JD006915. D19109.
Liu, Q., Boukabara, S., 2014. Community radiative transfer model (CRTM) applications in supporting the suomi national polar-orbiting partnership (SNPP) mission validation and verification. Remote Sens. Environ. Times 140, 744–754.
Liu, L., Li, Z., Yang, X., Gong, H., Li, C., Xiong, A., 2016. The long-term trend in the diurnal temperature range over Asia and its natural and anthropogenic causes. J. Geophys. Res. 121, 3519–3533. http://dx.doi.org/10.1002/2015JD024549.
Molod, A., Takacs, L., Suarez, M., Bacmeister, J., 2015. Development of the GEOS-5 atmospheric general circulation model: evolution from MERRA to MERRA2. Geosci. Model Dev. (GMD) 8, 1339–1356. http://dx.doi.org/10.5194/gmd-8-1339-2015.
Niu, F., Li, Z., Li, C., Lee, K.-H., Wang, M., 2010. Increase of wintertime fog in China: potential impacts of weakening of the Eastern Asian monsoon circulation and increasing aerosol loading. J. Geophys. Res. 115http://dx.doi.org/10.1029/2009JD013484. D00k20.
Petäjä, T., Järvi, L., Kerminen, V.-M., Ding, A.J., Sun, J.N., Nie, W., Kujansuu, J., Virkkula, A., Yang, X.-Q., Fu, C.B., Zilitinkevich, S., Kulmala, M., 2016. Enhanced air pollution via aerosol-boundary layer feedback in China. Sci. Rep. 6, 18998. http://dx.doi.org/10.1038/srep18998.
Qu, W., Wang, J., Gao, S., Wu, T., 2013. Effect of the strengthened western Pacific subtropical high on summer visibility decrease over eastern China since 1973. J. Geophys. Res. 118, 7142–7156.
Qu, W., Wang, J., Zhang, X., Yang, Z., Gao, S., 2015a. Effect of cold wave on winter visibility over eastern China. J. Geophys. Res. 120, 2394–2406.
Qu, W.J., Wang, J., Zhang, X.Y., Wang, D., Sheng, L.F., 2015b. Influence of relative humidity on aerosol composition: impacts on light extinction and visibility impairment at two sites in coastal area of China. Atmos. Res. 153, 500–511.
Quan, J., Gao, Y., Zhang, Q., Tie, X., Cao, J., Han, S., Meng, J., Chen, P., Zhao, D., 2013. Evolution of planetary boundary layer under different weather conditions, and its impact on aerosol concentrations. Particuology 11, 34–40. http://dx.doi.org/10.1016/j.partic.2012.04.005.
Randles, C.A., Silva, A.M.D., Buchard, V., Colarco, P.R., Darmenov, A., Govindaraju, R., Smirnov, A., Holben, B., Ferrare, R., Hair, J., Shinozuka, Y., Flynn, C.J., 2017. The MERRA-2 aerosol reanalysis, 1980 onward. Part I: system description and data assimilation evaluation. J. Clim. 30 (17), 6823–6850.
Robock, A., 1988. Enhancement of surface cooling due to forest fire smoke. Science 242, 911–913.
Seidel, D.J., Ao, C.O., Li, K., 2010. Estimating climatological planetary boundary layer heights from radiosonde observations: comparison of methods and uncertainty analysis. J. Geophys. Res. 115http://dx.doi.org/10.1029/2009JD013680. D16113.
Sun, Y.L., Wang, Z.F., Fu, P.Q., Jiang, Q., Yang, T., Li, J., Ge, X.L., 2013. The impact of relative humidity on aerosol composition and evolution processes during wintertime in Beijing, China. Atmos. Environ. 77, 927–934.
Sun, Y., Jiang, Q., Wang, Z., Fu, P., Li, J., Yang, T., Yin, Y., 2014. Investigation of the sources and evolution processes of severe haze pollution in Beijing in January 2013. J. Geophys. Res. 119. http://dx.doi.org/10.1002/2014JD021641.
Ten Hoeve, J.E., Augustine, J.A., 2015. Aerosol effects on cloud cover as evidenced by ground-based and space- based observations at five rural sites in the United States. Geophys. Res. Lett. 42. http://dx.doi.org/10.1002/2015GL066873.
Twomey, S., 1977. The influence of pollution on the short-wave albedo of clouds. J. Atmos. Sci. 34, 1149–1152.
Wang, J., Christopher, S.A., 2006. Mesoscale modeling of Central American smoke transport to the United States: 2. Smoke radiative impact on regional surface energy budget and boundary layer evolution. J. Geophys. Res. 111http://dx.doi.org/10.1029/2005JD006720. D14S92.
Wang, J., Jacob, D.J., Martin, S.T., 2008. Sensitivity of sulfate direct climate forcing to the hysteresis of particle phase transitions. J. Geophys. Res. 113http://dx.doi.org/10.1029/2007JD009368. D11207.
Wang, W., Huang, J., Minnis, P., Hu, Y., Li, J., Huang, Z., Ayers, J.K., Wang, T., 2010. Dusty cloud properties and radiative forcing over dust source and downwind regions derived from A-Train data during the Pacific Dust Experiment. J. Geophys. Res. 115http://dx.doi.org/10.1029/2010JD014109. D00H35.
Wang, Y., Yang, Y., Zhao, N., Liu, C., Wang, Q., 2012. The magnitude of the effect of air pollution on sunshine hours in China. J. Geophys. Res. 117http://dx.doi.org/10.1029/2011JD016753. D00V14.
Wang, Y., Khalizov, A., Levy, M., Zhang, R., 2013. New Directions: light absorbing aerosols and their atmospheric impacts. Atmos. Environ. 81, 713–715. http://dx.doi.org/10.1016/j.atmosenv.2013.09.034.
Wang, F., Zhang, C., Peng, Y., Zhou, H., 2014. Diurnal temperature range variation and its causes in a semiarid region from 1957 to 2006. Int. J. Climatol. 34 (2), 343–354.
Wang, W., Sheng, L., Jin, H., Han, Y., 2015. Dust aerosol effects on cirrus and altocumulus clouds in Northwest China. J. Meteor. Res. 29 (5), 793–805.
Wang, H.J., Chen, H.P., 2016. Understanding the recent trend of haze pollution in eastern China: roles of climate change. Atmos. Chem. Phys. 16, 4205–4211.
Wang, J., Xing, J., Mathur, R., Pleim, J.E., Wang, S., Hogrefe, C., Gan, C.-M., Wong, D.C., Hao, J., 2016. Historical trends in $PM_{2.5}$-related premature mortality during 1990-2010 across the Northern Hemisphere. Environ. Health Perspect. http://dx.doi.org/10.1289/EHP298.
Wang, J., Xing, J., Wang, S., Hao, J., 2017a. The pathway of aerosol direct effects impact on air quality: a case study by using process analysis. Geophys. Res. Abstr. 19 EGU2017-8568.
Wang, J., Zhao, B., Wang, S., Yang, F., Xing, J., Morawska, L., Ding, A., Kulmala, M., Kerminen, V.-M., Kujansuu, J., Wang, Z., Ding, D., Zhang, X., Wang, H., Tian, M., Petäjä, T., Jiang, J., Hao, J., 2017b. Particulate matter pollution over China and the effects of control policies. Sci. Total Environ. 584–585, 426–447.
Xing, J., Mathur, R., Pleim, J., Hogrefe, C., Gan, C.-M., Wong, D.C., Wei, C., Wang, J., 2015. Air pollution and climate response to aerosol direct radiative effects: a modeling study of decadal trends across the northern hemisphere. J. Geophys. Res. Atmos. 120, 12221–12236.
Xing, J., Wang, J., Mathur, R., Pleim, J., Wang, S., Hogrefe, C., Gan, C.-M., Wong, D.C., Hao, J., 2016. Unexpected benefits of reducing aerosol cooling effects. Environ. Sci. Technol. 50, 7527–7534.
Xu, X., 2012. Spatiotemporal variation of total cloud and low cloud over China (in Chines with English abstract). Meteorol. Mon. 38 (1), 90–95.
Yan, L., Liu, X., Yang, P., Yin, Z.Y., North, G.R., 2011. Study of the impact of summer monsoon circulation on spatial distribution of aerosols in East Asia based on numerical simulations. Journal of Applied Meteorology and Climatology 50, 2270–2282.
Yang, X., Zhao, C., Guo, J., Wang, Y., 2016. Intensification of aerosol pollution associated with its feedback with surface solar radiation and winds in Beijing. J. Geophys. Res. Atmos. 121, 4093–4099. http://dx.doi.org/10.1002/2015JD024645.
Ye, J., Li, F., Sun, G., Guo, A., 2010. Solar dimming and its impact on estimating solar radiation from diurnal temperature range in China, 1961–2007. Theor. Appl. Climatol. 101, 137–142.
Yin, Z., Wang, H., 2015. The relationship between the subtropical western pacific SST and haze over north-Central north China plain. Int. J. Climatol. 36, 3479–3491.
Yu, H., Kaufman, Y.J., Chin, M., Feingold, G., Remer, L.A., Anderson, T.L., Balkanski, Y., Bellouin, N., Boucher, O., Christopher, S., DeCola, P., Kahn, R., Koch, D., Loeb, N., Reddy, M.S., Schulz, M., Takemura, T., Zhou, M., 2006. A review of measurement-based assessments of the aerosol direct radiative effect and forcing. Atmos. Chem. Phys. 6, 613–666.
Zhang, X.Y., Sun, J.Y., Wang, Y.Q., Li, W.J., Zhang, Q., Wang, W.G., Quan, J.N., Cao, G.L., Wang, J.Z., Yang, Y.Q., Zhang, Y.M., 2013. Factors contributing to haze and fog in China (in Chinese with English abstract). Chin. Sci. Bull. 58, 1178–1187.
Zhang, R.H., Li, Q., Zhang, R.N., 2014. Meteorological conditions for the persistent severe fog and haze event over eastern China in January 2013. Sci. China Earth Sci. 57, 26–35.
Zhang, Y., Ding, A., Mao, H., Nie, W., Zhou, D., Liu, L., Huang, X., Fu, C., 2016. Impact of synoptic weather patterns and inter-decadal climate variability on air quality in the North China Plain during 1980–2013. Atmos. Environ. 124, 119–128.
Zhao, P.S., Dong, F., He, D., Zhao, X.J., Zhang, X.L., Zhang, W.Z., Yao, Q., Liu, H.Y., 2013a. Characteristics of concentrations and chemical compositions for $PM_{2.5}$ in the region of Beijing, Tianjin, and Hebei, China. Atmos. Chem. Phys. 13, 4631–4644. http://dx.doi.org/10.5194/acp-13-4631-2013.
Zhao, X.J., Zhao, P.S., Xu, J., Meng, W., Pu, W.W., Dong, F., He, D., Shi, Q.F., 2013b. Analysis of a winter regional haze event and its formation mechanism in the North China Plain. Atmos. Chem. Phys. 13, 5685–5696.
Zhou, Y., Ren, G., 2011. Change in extreme temperature event frequency over mainland China, 1961 – 2008. Clim. Res. 50, 125–139. http://dx.doi.org/10.3354/cr01053.
Zhu, J.L., Liao, H., Li, J.P., 2012. Increases in aerosol concentrations over eastern China due to the decadal-scale weakening of the East Asian summer monsoon. Geophys. Res. Lett. 39http://dx.doi.org/10.1029/2012GL051428. L09809.
Zou, J., Sun, J., Ding, A., Wang, M., Guo, W., Fu, C., 2017. Observation-based estimation of aerosol-induced reduction of planetary boundary layer height. Adv. Atmos. Sci. 34, 1–12.